



Carbon materials derived from chitosan/cellulose cryogel-supported zeolite imidazole frameworks for potential supercapacitor application



Zehui Li^{a,b,c,1}, Lan Yang^{d,1}, Hongbin Cao^a, Yu Chang^e, Kexin Tang^a, Zhiqin Cao^a, Junjun Chang^{a,c}, Youpeng Cao^a, Wenbo Wang^{a,c}, Meng Gao^c, Chenming Liu^{a,*}, Dagang Liu^e, He Zhao^a, Yi Zhang^a, Mingjie Li^{f,*}

^a Beijing Engineering Research Center of Process Pollution Control, Division of Environmental Technology and Engineering, Institute of Process Engineering, Chinese Academy of Sciences, Beijing 100049, China

^b State Key Joint Laboratory of Environment Simulation and Pollution Control, School of Environment, Tsinghua University, Beijing 100084, China

^c University of Chinese Academy of Sciences, Beijing 100049, China

^d Environmental Research Academy, North China Electric Power University, Beijing 102206, China

^e School of Environmental Science and Engineering, Nanjing University of Information Science and Technology, Nanjing, 210044, China

^f Qingdao Institute of Biomass Energy and Bioprocess Technology, Chinese Academy of Sciences, Qingdao 266101, China

ARTICLE INFO

Article history:

Received 8 May 2017

Received in revised form 18 July 2017

Accepted 30 July 2017

Available online 1 August 2017

Keywords:

Chitosan

Cellulose

Carbon cryogel

Zeolite imidazole frameworks

Supercapacitor

ABSTRACT

In order to promote sustainable development, green and renewable clean energy technologies continue to be developed to meet the growing demand for energy, such as supercapacitor, fuel cells and lithium-ion battery. It is urgent to develop appropriate nanomaterials for these energy technologies to reduce the volume of the device, improve the efficiency of energy conversion and enlarge the energy storage capacity. Here, chitosan/cellulose carbon cryogel (CCS/CCL) were designed and synthesized. Through the introduction of zeolite imidazole frameworks (ZIFs) into the chitosan/cellulose cryogels, the obtained materials showed a microstructure of ZIF-7 (a kind of ZIFs) coated chitosan/cellulose fibers (CS/CL). After carbonizing, the as-prepared carbonized ZIF-7@cellulose cryogel (NC@CCL, NC is carbonized ZIF-7) and carbonized ZIF-7@chitosan cryogel (NC@CCS) exhibited suitable microspore contents of 34.37% and 30%, respectively, and they both showed an internal resistance lower than 2 Ω. Thereby, NC@CCL and NC@CCS exhibited a high specific capacitance of 150.4 F g⁻¹ and 173.1 F g⁻¹, respectively, which were much higher than those of the original materials. This approach offers a facile method for improving the strength and electronic conductivity of carbon cryogel derived from nature polymers, and also efficiently inhibits the agglomeration of cryogel during carbonization in high temperature, which opens a novel avenue for the development of carbon cryogel materials for application in energy conversion systems.

© 2017 Elsevier Ltd. All rights reserved.

1. Introduction

Fossil energy has been consumed rapidly in the last hundred years, especially twenty-first century (York & York, 2012). In order to deal with the energy crisis, people pay more and more attentions to energy saving, as well as the developing of new energy storage and conversion systems. Some renewable energy devices such as supercapacitor, fuel cell, and solar cell, etc, are gradually warming up (Snook, Kao & Best, 2011; Zhou et al., 2016). On the whole, the supercapacitor has the characteristics of high power density, short charging time and long service life (Peng et al., 2017; Yu, Tetard, Zhai & Thomas, 2015). It can be divided into two kinds,

electric double layer capacitor (EDLC) and pseudocapacitance. The former can form potential to store energy through the interface between positive and negative ions in the adsorption of electrolyte and electrode with no electrochemical reaction, while the latter stores energy through electrochemical reaction on the electrode material (Li et al., 2014; Yang et al., 2017). Nowadays, both kinds of capacitors have wide application potentials in the field of power system and vehicle.

Carbon materials are the most widely used electrode materials for supercapacitors, including activated carbon, carbon nanotubes, graphene, carbon nanofiber and carbon cryogel, etc. (Foresti, Vazquez & Boury, 2017; Lang, Hirata, Fujita & Chen, 2011; Zhai et al., 2012). Since they have high specific surface areas (SSA), suitable pore size and good electrical conductivity. As a new type of nanoporous carbon materials, carbon cryogel derived from carbohydrate polymers such as cellulose (CL), chitosan (CS) is

* Corresponding authors.

E-mail addresses: chmliu@ipe.ac.cn (C. Liu), limj@qibebt.ac.cn (M. Li).

¹ Joint first author: Zehui Li and Yang Lan contributed equally to this work.

environmental friendly, and owns high conductivity and thermal stability, which is an ideal electrode material for energy storage (Frindy et al., 2017; Wan & Li, 2017; You, Li, Ding, Wu & Li, 2017). However, such nanoporous carbon materials are easy to agglomerate during pyrolysis because of the loss of oxygen-containing groups in high temperature. Consequently, their applications in energy storage is inhibited because the electrons cannot transport efficiently (Wei et al., 2015). Recently, introducing hard templates is an important way to improve the structure stability in preparation of carbon cryogels through carbonizing carbohydrates. It was also found that the morphology, pore structure, the degree of crystallization and electrochemical the chemical and physical properties of carbon cryogels can be modulated by doping heteroatom or metal ions. For example, by introducing metal into the carbon cryogel can adjust the morphology, pore structure, and the degree of crystallization, thereby tune their electrochemical activity and conductivity (Tian, 2017; Wei, Wan & Gao, 2016).

Zeolite imidazole frameworks (ZIFs) is a kind of new metal zeolite topologies by complexing transition metal ions with imidazole ligand. Such structure owns the characters of high stability and high porosity, which are usually used as hard templates in preparing carbon materials. In addition, the electrical conductivity of the ZIFs materials can be enhanced through pyrolysis, and ZIFs after pyrolysis regarded as ideal materials for supercapacitor electrode (Yao & Wang, 2014; Zhu & Dong, 2013). For instance, (Gao et al., 2014) have prepared a kind of novel carbon nanomaterials by pyrolyzing ZIF-8 under inert gas. The resultant nanocarbons exhibited tunable properties like particle size, microtexture, and SSA, thereby optimal capacitive properties could be achieved e.g. specific capacitance up to 130 F g^{-1} .

In this work, chitosan cryogel was used as a basic material, then ZIF-7 was added into the cryogel and carbonized at 950°C , the resultant material was prepared as electrode for supercapacitors, and the specific capacitance is studied in details. As contrast, cellulose cryogel, ZIF-8 and ZIF-67 were used to substitute for chitosan and ZIF-7.

2. Experiment section

2.1. Sample preparation

2.1.1. Preparation of cryogel materials

5 g of raw cellulose powder and 1 L deionized water were poured into a beaker and stirred overnight to make the powder fully swollen. The suspension was polished through a wet-ginder (Labor-Pilot 2000/4, IKA Works, Inc.) with a milling gap of less than 0.1 mm at a flow rate of 10 L h^{-1} for 10 cycles. After that, the cellulose solution was homogenized 10 times through a high pressure homogenizer (M-100P, Microfluidics Co., USA) with a pressure of 250 MPa. The obtained gel was further freezing dried to obtain cellulose nanofiber cryogel, which named as CL cryogel. (Liu, Li, Zhu, Li & Kumar, 2014) Chitosan nanofiber cryogel was prepared by the same way and the obtained sample was labeled CS cryogel. CCL and CCS cryogel were collected after carbonizing CL and CS at 950°C under Ar gas.

2.1.2. Preparation of carbonized ZIF-7

0.3 g of $\text{Zn}(\text{NO}_3)_2 \cdot 6\text{H}_2\text{O}$ (molecular weight: 297.51) and 0.36 g benzimidazole (bIM, molecular weight: 118.14, mole ratio: 0.33) were dissolved in 30 mL methanol, separately. Subsequently, $\text{Zn}(\text{NO}_3)_2$ solution was added into the bIM solution and stirring for 3 h. After centrifugation (8000 rpm, 3 min), the precipitate was collected and washed by methanol for 3 times. Finally, ZIF-7 was obtained after drying, and NC was got after pyrolysis at 950°C under Ar gas, and acid wash with 2 M HCl.

2.1.3. Preparation of carbon cryogel materials

0.3 g $\text{Zn}(\text{NO}_3)_2 \cdot 6\text{H}_2\text{O}$ mixed with 0.2 g CS cryogel in 30 mL methanol and stirring for 4 h. Subsequently, the mixture was added into 30 mL benzimidazole solution (0.36 g) and stirring for 3 h. After that, the precipitate was collected by centrifugation (8000 rpm, 3 min) and washed with methanol, the dried sample named ZIF-7@CS. The ZIF-7@CS was further carbonized under 950°C in Ar gas and washed with 2 M HCl. The resultant sample was named as NC@CCS carbon cryogels.

ZIF-7@CL and NC@CCL were prepared like ZIF-7@CS and NC@CCS especially using CL instead of CS.

ZIF-8@CS, NC-8@CCS, ZIF-67@CS and NC-67@CCS were prepared like ZIF-7@CS and NC@CCS especially using ZIF-8 and ZIF-67 instead of ZIF-7.

2.2. Characterization

The morphology of samples were characterized by thermal field emission scanning electron microscopy (SEM, JSM-7001F, JEOL) and transmission electron microscopy (TEM, JEM-2100F, JEOL). The structure of samples were characterized by X-ray diffraction (XRD, SmartLab-9, Rigaku), X-ray photoelectron spectroscopy (XPS, ESCALAB 250Xi, Thermo Fisher Scientific), nitrogen isotherm (77 K) physisorption (Quantachrome Autosorb iQ) surface analyser and Raman spectroscopy (Renishaw Raman system, inVia-Reflex).

The acceleration voltage of SEM is 5 kV, while that of TEM is 200 kV. Before TEM test, the sample needs to be pretreated, the sample is dissolved in ethanol and dispersed by ultrasonic, then the solution was dropped on the micro grid with copper net.

Grating of XRD use $\text{CuK}\alpha$ ($\lambda = 0.15406 \text{ nm}$), and the scaning range of 2θ is 5–90°.

Before XPS test, the sample should be spread on the aluminum foil with double faced adhesive tape, then the sample was flattened and cut into the size of $4 \text{ mm} \times 4 \text{ mm}$ to be tested. Spot size of X-ray is $500 \mu\text{m}$.

The pore structures were characterized by nitrogen isotherm physisorption. The samples were degassed at 120°C for 12 h before measuring. The internal SSA of sample was calculated according to the Brunauer-Emmett-Teller (BET) method based on the adsorption data in a relative pressure range of 0.05–0.35. The micropore volume and surface information were analyzed by the V-t method. The pore size distribution (PSD) was measured by the Discrete-Fourier-Transformation (DFT) method.

Raman spectroscopy was measured by the exciting source of 20 mW air-cooled argon ion laser with wavelength of 532 nm, laser diameter was 1 mm, and laser power at the sample position was 4.0 mW. The data acquisition time was set to 10 s.

2.3. Electrochemical measurements

Electrochemical measurements of materials were tested under an Autolab electrochemical workstation (PGSTAT302N, Metrohm). Cyclic voltammetry (CV), electrochemical impedance spectroscopy (EIS) and galvanostatic charge-discharge (GCD) were tested in a standard three-electrode system. CV was scanned from 10, 20, 50, 100–200 mV s^{-1} , and EIS was measured under open-circuit potential with signal amplitude of 10 mV and frequency from 10^5 to 10^{-2} Hz in $0.1 \text{ M KCl} + 10 \text{ mM Fe}(\text{CN})_6^{3-/4-}$ (1:1 mixture) solution. GCD was under current density of 1 A g^{-1} . Counter electrode was platinum plate ($1 \times 1 \text{ cm}^2$), and reference electrode was mercury/mercuric oxide electrode (Hg/HgO , 1 M KOH), working electrode was constituted by dropping slurry onto nickel foams ($1 \times 1 \text{ cm}^2$, 10 MPa) and pressing after drying, and 6 M KOH aqueous solution (about 25°C) was used as electrolyte. The slurry was prepared by mixing 80 wt% of active material, 10 wt% of carbon black, and 10 wt% of polyacrylonitrile in N-methyl-2-pyrrolidone solvent.

Then, the slurry was cast on Ni foam ($1 \times 1 \text{ cm}^2$) to achieve a loading capacity of 2 mg cm^{-2} .

In the GCD curve measured by three electrode system, the mass ratio capacitance is calculated by the following formula:

$$C_s = I\Delta t/m\Delta E$$

While C_s (F g^{-1}) is the specific capacitance, I (A) is charge-discharge current, Δt (s) is discharge time, m (g) is the quality of active material in the working electrode, ΔE (V) is voltage changes during the discharge process.

3. Results and discussion

3.1. Physicochemical characterization

Scheme 1 illustrates the preparation procedure of NC@CCL and NC@CCS. Firstly, the CL and CS cryogels with film and fibrous porous structure were prepared. Secondly, ZIF-7 was added into CL and CS cryogels. Due to the strong coordination interaction between rich oxygen-containing functional groups from CL and CS cryogel and metal ions from ZIF-7 (Zn(II)), ZIF-7 particles could easily be attached on the CL and CS to form sandwich and coral structure. Thirdly, the as-received cryogels were converted to carbon materials with suitable microspore contents, nitrogen contents, and nanoporous structure.

Fig. 1 shows the SEM images of the synthesized NC, NC@CCL and NC@CCS. It can be seen that the NC material derived from ZIF-7 (**Fig. 1a**) is discrete ellipsoidal particles, with a size of 500 nm to $\sim 5 \mu\text{m}$. The fold layer structure of CCL cryogel (**Fig. 1b**) is about $1 \mu\text{m}$ in thickness, and the porous layer structure of CCS cryogel (**Fig. 1c**) is much thinner with many fibers and pores. After adding ZIF-7 into CL cryogel and carbonizing, sandwich structure in which NC wrap up CCL can be seen (**Fig. 1d**). Scattered NC particles are homogeneously distributed on the surface of the fiber layer, forming a three-dimensional porous structure. However, there are still many CCL fibers exposed, indicating that the oxygen-containing functional groups in CL are not abundant. Similarly, the coral structure could be seen (**Fig. 1e**) after adding ZIF-7 into CS cryogel and carbonizing. Abundant slim fibers of CCS cryogel can make the NC particles well covered on the outer layer of CCS cryogel, thus forming abundant pores. At the same time, the magnified image can be seen in **Fig. 1f**, NC well composited with CCS cryogel and gathered on CCS fiber to form a bead structure, indicating that the chelation or electrostatic adsorption effect between rich oxygen-containing functional groups on the surface of CCS fibers and Zn(II) ion in ZIF-7.

The morphologies of materials were further explored from nanoscale, and **Fig. 2** shows the TEM images of the materials. NC (**Fig. 2a,d**) is amorphous carbon with obscure crystal structure. The CCL cryogel is lamellar and the size is much larger than that of NC (**Fig. 2b,e**), and NC particles are inclined to bind with the folds of CCL during the compounding process. Because the folds contain majority of oxygen-containing functional groups, which can chelate the Zn(II) ions in the ZIF-7. The diameter of single fiber in CCS cryogel is about several nanometers to tens of nanometers, which is much less than NC. When NC is combined with CCS cryogel (**Fig. 2c,f**), NC can easily cover the fibers of CCS, and form a bead-like structure. Such structure of CCS can have higher SSA and expose more active sites than that of CCL. Thus CCS can be combined with ZIF-7 easily.

The pore structure of the materials was further investigated by nitrogen adsorption-desorption isotherm. As shown in **Fig. 3a**, the typical type-IV curve is observed for the materials. The SSA was calculated by BET method, and the SSA of carbonized NC, CCL and CCS was $1085.6 \text{ m}^2 \text{ g}^{-1}$, $459.727 \text{ m}^2 \text{ g}^{-1}$ and $357.414 \text{ m}^2 \text{ g}^{-1}$. After compositing with CCL and CCS, SSA of NC@CCL and NC@CCS decreased to $285.4 \text{ m}^2 \text{ g}^{-1}$ and $285.2 \text{ m}^2 \text{ g}^{-1}$. The decrease of SSA indicated

that the chelation reaction between Zn(II) in ZIF-7 and oxygen containing functional groups may cause blockage of some channels. The pore size distribution of the materials were calculated by DFT method. As shown in Table S1, the microspore contents of NC, CCL and CCS are 46.24%, 41.86% and 15.46%. After compositing with CL and CS and carbonization, it changes to 34.37% and 30%, respectively. It is well known that the mesoporous ($>2 \text{ nm}$) channels and uniform pore sizes between 3 nm to 5 nm are required to improve the capacitance of EDLC (Du, Guo, Song & Chen, 2010). Therefore, the ratio of microspore content of NC@CCL and NC@CCS decreased with the increase of mesopores, which is benefit for improving the storage efficiency. Notably, although CCS has the most mesopores, too less microspore may introduce the material hard to activity.

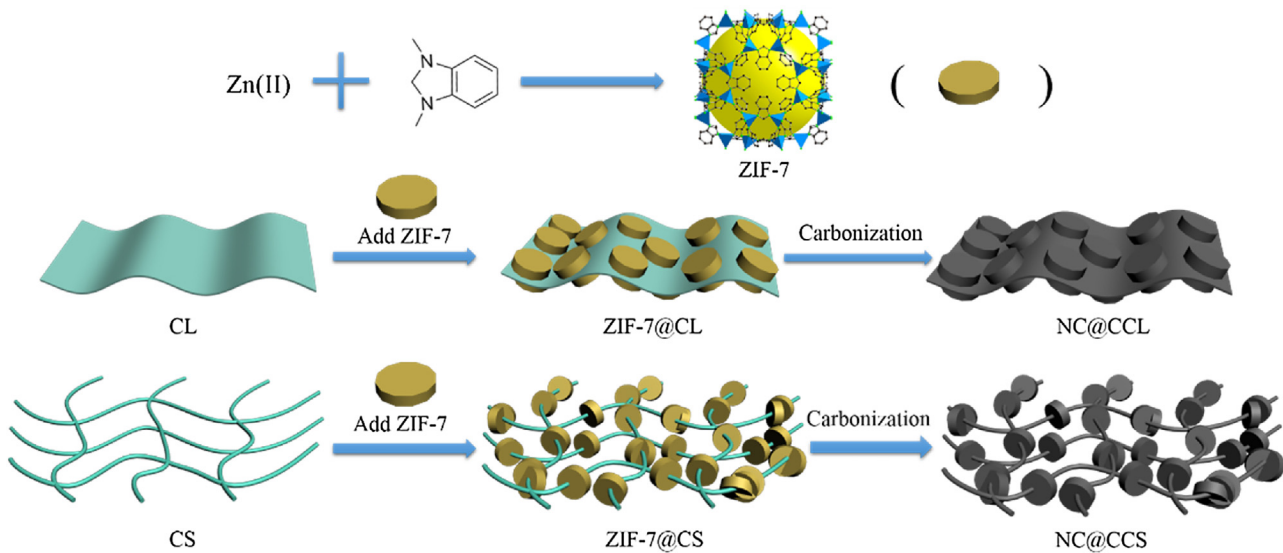
The Raman spectrum can be used to characterize the defects of the materials and the hybridization of carbon. As shown in **Fig. 3c**, three peaks at around 1340 , 1590 and 2850 cm^{-1} are observed, corresponding to the characteristic D peak, G peak and 2D satellite peak of carbon. Among them, the I_D/I_G of NC is 0.93, while those of NC@CCL and NC@CCS are 0.90 and 0.85, which indicates that the composite of CL and CS can increase sp^2 hybridization and the number of unsaturated carbon atoms.

XRD is used to further verify the crystal structure and the graphitization degree. As shown in **Fig. 3d**, all samples show two broad diffraction peaks at the position of 24° and 43° , corresponding to C(002) surface and C(100) surface. Among them, C(002) crystal surface indicates that the degree of graphitization, whose higher intensity refers to a higher degree of graphitization and a less content of single layer graphite. Therefore, NC@CCS gives the highest degree of graphitization. This attributes to the addition of the CS cryogel, leading to a decrease in the number of non-parallel graphene in the material. It is consistent with the results of Raman. In addition, the diffraction peak of Zn atom was not found, indicating that the Zn atom in NC is almost removed during the pickling process.

Fourier transform infrared spectroscopy (FT-IR) of NC, CCL, CCS, NC@CCL and NC@CCS are provide evidence for the characteristic vibrations of the attached groups. As shown in **Fig. S1**, the intensity of peaks in NC was much lower than that of other materials at the range between 1000 – 1500 cm^{-1} , indicating that almost no oxygen-containing functional groups still existed in this organic framework. For CCL and CCS, the bands at 1372 and 1320 cm^{-1} suggested the existence of hydroxyl groups in cellulose and chitosan (Qiu et al., 2010). The peak at 1621 cm^{-1} increased after NC coated with CCL or CCS, attributing to the C=C vibration between ZIF-7 and CL/CS (Gao, Hai, Baigude, Guan, & Liu, 2016). In addition, an obvious peak at 1160 cm^{-1} of NC@CCS should be attributed to the presence of C–N stretching vibrations (Fazlifard, Mohammadi, & Bakhtiari, 2017) originating in amino group of chitosan.

XPS shows the chemical structure on the surface of the materials. As shown in **Fig. 4a**, XPS wide spectrum displays the surface of all samples with Zn, C, N, O elements. As listed in Table S2, the contents of C, N and O in the NC@CCS are 89.82%, 5.62% and 4.56%, respectively. Compared to that of NC, the content of N and O are increased with the decrease of C content. This is related to the abundant content of N and O in the raw material of CS cryogel itself. On the contrary, the CL cryogel does not have nitrogen content, so the nitrogen content of the NC@CCL decreases obviously. At the same time, the change of NC@CCS is smaller than that of NC@CCL, indicating that the extent of ZIF-7 wrapped on CS is higher than CL.

High-resolution C 1s and N 1s spectra are further analyzed. As shown in **Fig. 4b,c** and Fig. S2, 284.8 eV , 286 eV , 286.7 eV and 288.5 eV peaks in C 1s spectra corresponds to C–C/C=C (sp^3 hybridization), C–N, C–O–C and C=O. It can be found that the content of C–O–C increases obviously, which stems from the abundant oxygen-containing functional groups in CL and CS. The peaks at 398.4 eV , 400 eV , 401 eV and 402.8 eV in the N 1s



Scheme 1. Schematic illustration of the synthesis process for the NC@CCL and NC@CCS.

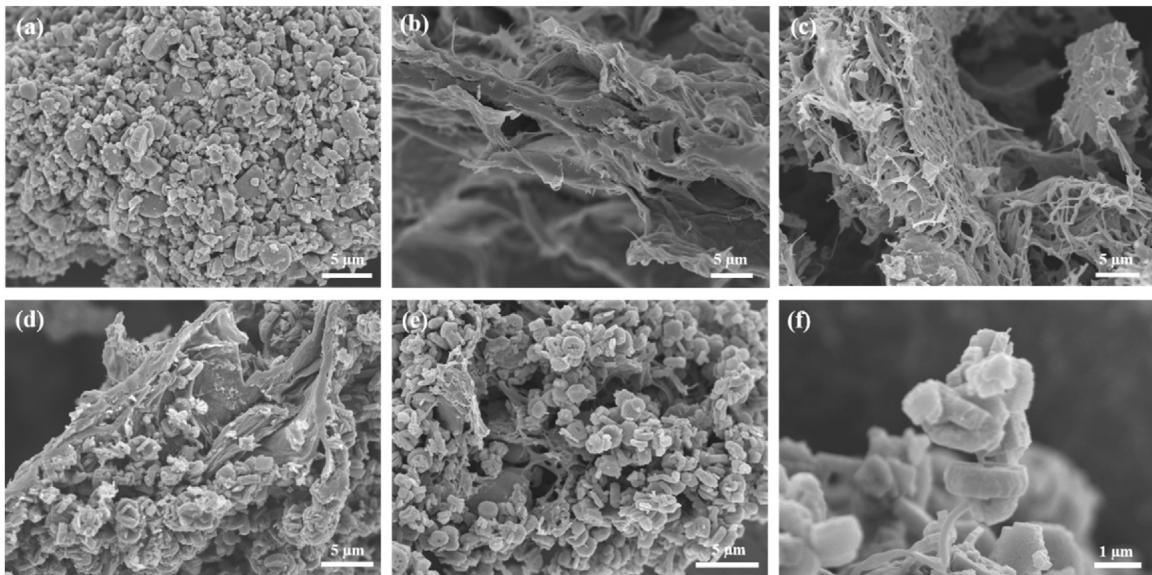


Fig. 1. SEM of (a) NC, (b) CCL, (c) CCS, (d) NC@CCL and (e,f) NC@CCS.

spectra, corresponding to the pyridine-nitrogen, pyrrolic-nitrogen, graphite-nitrogen and nitrogen-oxides, respectively. Compared with NC, CCL and CCS, the ratios of pyridine-nitrogen and graphite-nitrogen to total nitrogen in NC@CCS are higher. And it has been reported that this two kinds of nitrogen have direct effect on the electrochemical properties (Guo, 2016).

3.2. Electrochemical performance

The capacitive performance of the materials was studied by CV. The CV curves of NC, NC@CCL and NC@CCS electrodes at a scan rate of 10 mV s^{-1} – 200 mV s^{-1} are shown in Fig. 5a–c, respectively. The CV curves of all samples present a class of quasi-rectangular shape with no redox peak, demonstrating good EDLC performance. The rectangle shape of NC@CCS is more obvious, even under the large sweep speed 200 mV s^{-1} . The shape is still deformation, showing the ideal supercapacitance and fast charging and discharging performance. In addition, under the same sweep rate, the current density of NC@CCS is larger than NC@CCL and NC, indicating that

the combination of CS cryogel and ZIF-7 can increase the capacitance and current to a certain extent.

The specific capacitance of the material is determined by GCD measurement. As shown in Fig. 5d, NC, CCL, CCS, NC@CCL and NC@CCS electrodes are tested under the current density of 1 A g^{-1} , giving a typical triangular shape (left is charging part, right is discharge part). It can be seen that the charging and discharging part are symmetric, with no obvious ohmic drop, showing stable electrochemical performance and small internal resistance. According to the formula of calculating C_s , the specific capacitance of NC, CCL, CCS, NC@CCL and NC@CCS electrode are 14.6 F g^{-1} , 79.1 F g^{-1} , 86.8 F g^{-1} , 150.4 F g^{-1} and 173.1 F g^{-1} . Compared to the NC, CCL cryogel and CCS cryogel, C_s of NC@CCL and NC@CCS was improved to a great extent, which can be attributed to the new pore structure formed by ZIF-7 and nanofibers. Table 1 gives the comparison of the specific capacitance of different nanoporous carbon materials reported in recent years. It can be seen that the performance of NC@CCL and NC@CCS electrodes has obvious advantages over others.

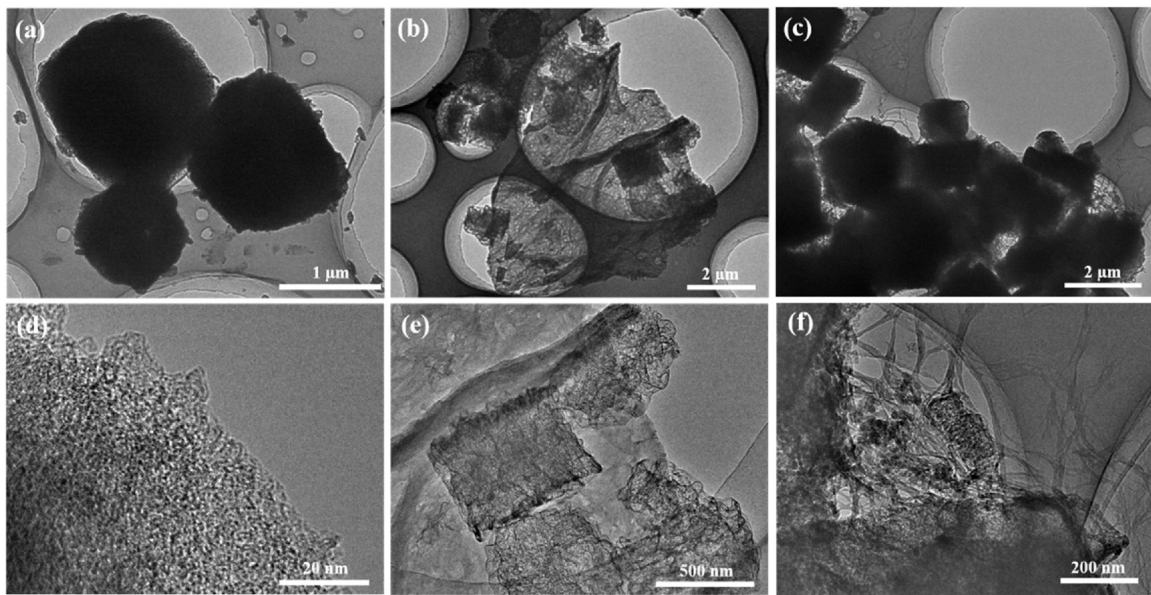


Fig. 2. TEM of (a) NC, (b) NC@CCL, (c) NC@CCS and corresponding (d,e,f) high-resolution TEM images.

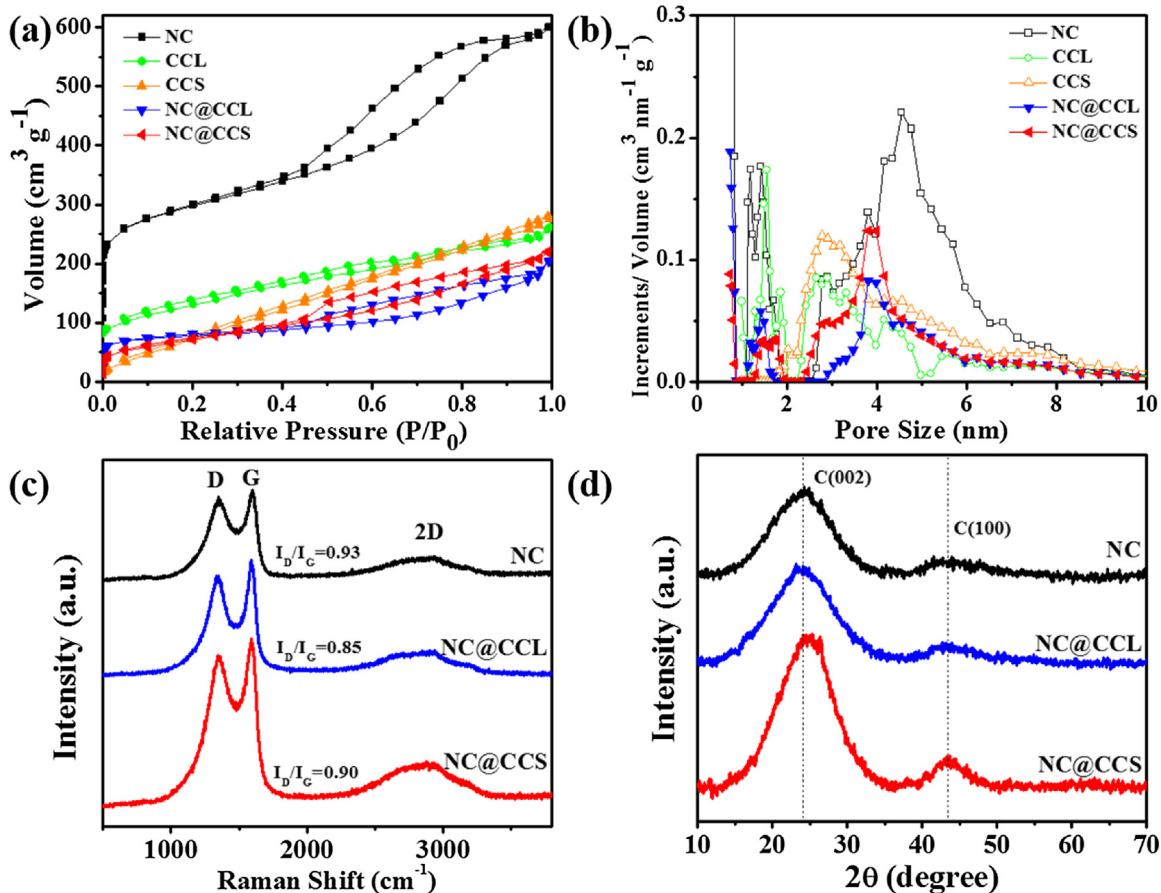


Fig. 3. Characterizations of NC, NC@CCL and NC@CCS: (a) N_2 adsorption-desorption isotherms at 77 K, (b) pore-size distributions, (c) Raman spectra, and (d) wide-angle XRD patterns.

The resistance of electrode materials can be further understand by EIS. As shown in Fig. 6a, EIS images of NC, NC@CCL and NC@CCS electrodes are semicircle in the high-frequency region and line in the low-frequency region. The equivalent circuit is a series circuit, in which the intercept of the semicircle (high frequency area) on

the real axis is the solution resistance (R_Ω), and the radius of the semicircle is internal resistance (R_{ct}) of work electrode. The calculated R_{ct} of NC, NC@CCL and NC@CCS are 3.5 Ω , 1.5 Ω , and 2 Ω , respectively. Conversely, obvious semicircle can be seen during all frequency region of CCL and CCS, indicating a poor electroconduc-

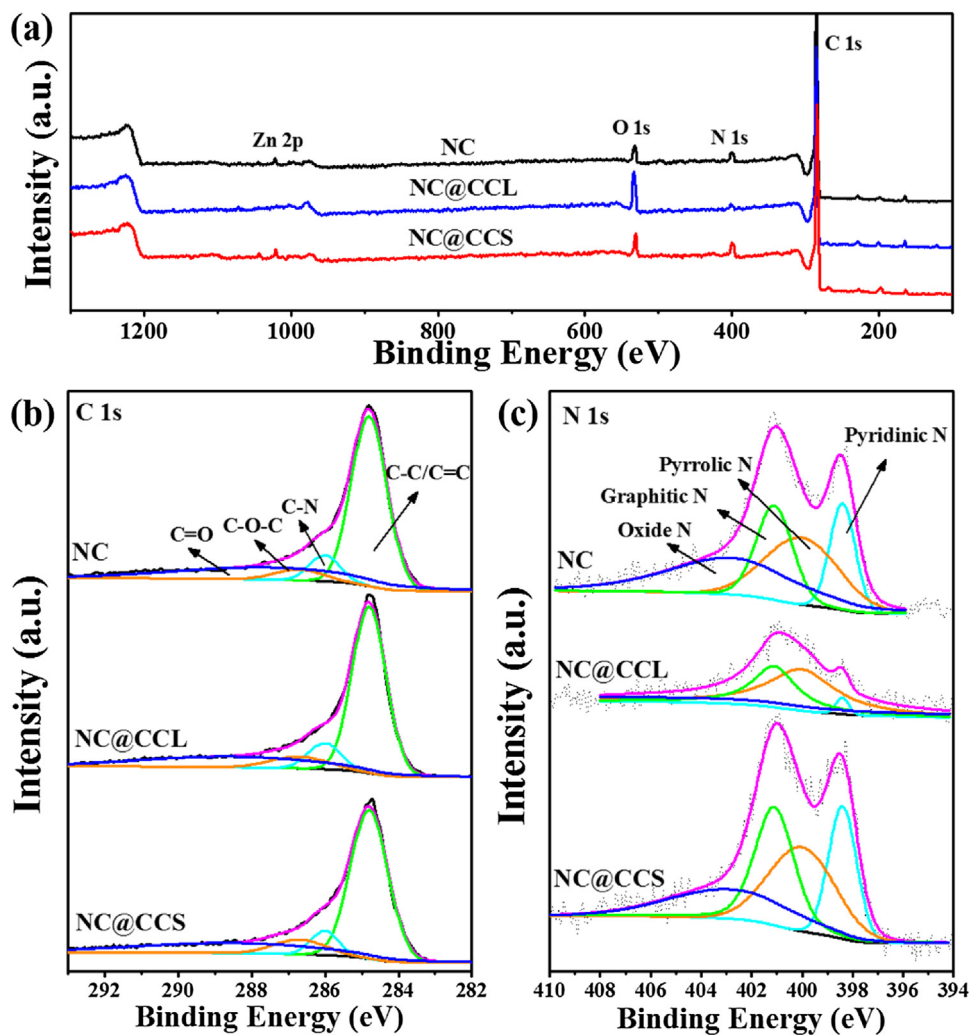


Fig. 4. (a) XPS full spectra and high-resolution XPS spectra of (b) C 1s and (c) N 1s.

Table 1

The capacitive performance of nanoporous carbon materials in recent literatures.

Electrode materials	Specific capacitance (F g^{-1})	Electrolyte	Current load/scan rate	References
NC@CCL	150.4	6 M KOH	1 A g^{-1}	This work
NC@CCS	173.1	6 M KOH	1 A g^{-1}	This work
ZIF-8-800 ^a	130	0.5 M H_2SO_4	50 mV s^{-1}	(Chaikittisilp et al., 2012)
CZIF69a ^b	168	0.5 M H_2SO_4	5 mV s^{-1}	(Wang et al., 2013)
K700 ^c (porous carbon aerogel)	142.1	6 M KOH	0.5 A g^{-1}	(Hao et al., 2014)
Carbon-L-950 ^d	178	6 M KOH	10 A g^{-1}	(Zhang, Sun, Shen & Cao, 2014)
N-doped graphene-based hierarchical porous carbon aerogel	197	6 M KOH	0.2 A g^{-1}	(Hao et al., 2015)
GNPC(ZIF-8/GO) ^e	144	6 M KOH	0.1 A g^{-1}	(Jiang, Sun & Xu, 2016)
ZIF-8/CNTs ^f	185	1 M Na_2SO_4	0.5 A g^{-1}	(Zhang et al., 2016)
cellulose/PANI conductive hydrogels	145	1 M H_2SO_4	0.1 A g^{-1}	(Tian et al., 2017)

^a ZIF-8-800: carbonized ZIF-8 at 800 °C under nitrogen gas.

^b CZIF69a: activated carbonized ZIF-69 (a kind of ZIFs).

^c K700: carbonized cellulose aerogels at 700 °C.

^d Carbon-L-950: carbonized ZIF-7/glucose composite at 950 °C.

^e GNPC(ZIF-8/GO): 2D sandwich-like ZIF-8 derived graphene-based N-doped porous carbons.

^f ZIF-8/CNTs: ZIF-8/carbon nanotubes.

tivity of these materials. The result is related to the structure of carbon cryogel, as a kind of conductive material, NC can reduce the internal resistance after compositing with the CCL and CCS cryogels. The long-cycle stability of NC@CCS is also evaluated by GCD

at 8 A g^{-1} (Fig. 6b). Even after 1000 cycles, the capacitance can still retain over 95.5%, indicating that the excellent cycling stability.

The capacitance of other ZIFs materials and CS cryogel composites can be further explored. As shown in Fig. S3, ZIF-8 and ZIF-67 are composites with CS and carbonized as NC-8@CCS and NC-67@CCS,

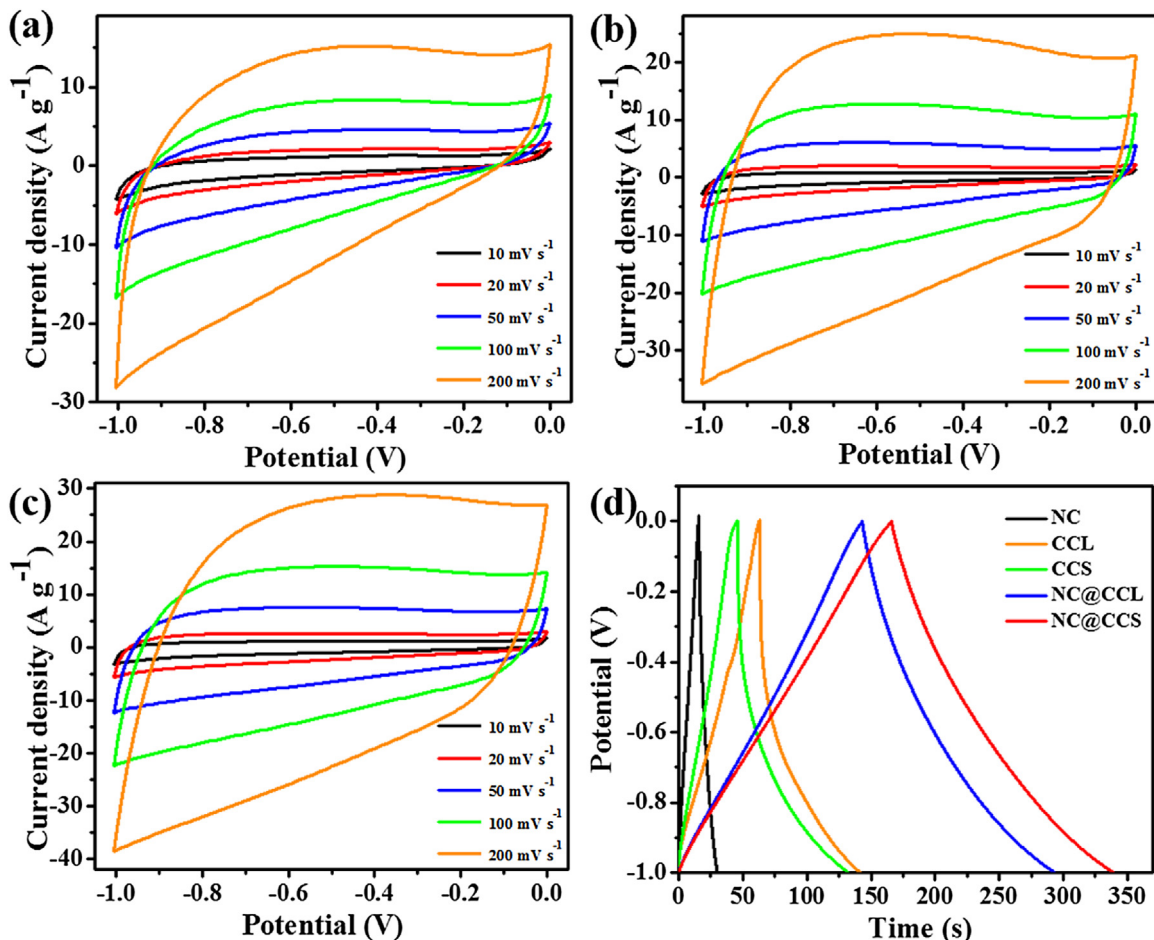


Fig. 5. CV curves at different scan rates of (a) NC, (b) NC@CCL and (c) NC@CCS; (d) GCD curves at a current density of 1 A g^{-1} of NC, CCL, CCS, NC@CCL, and NC@CCS.

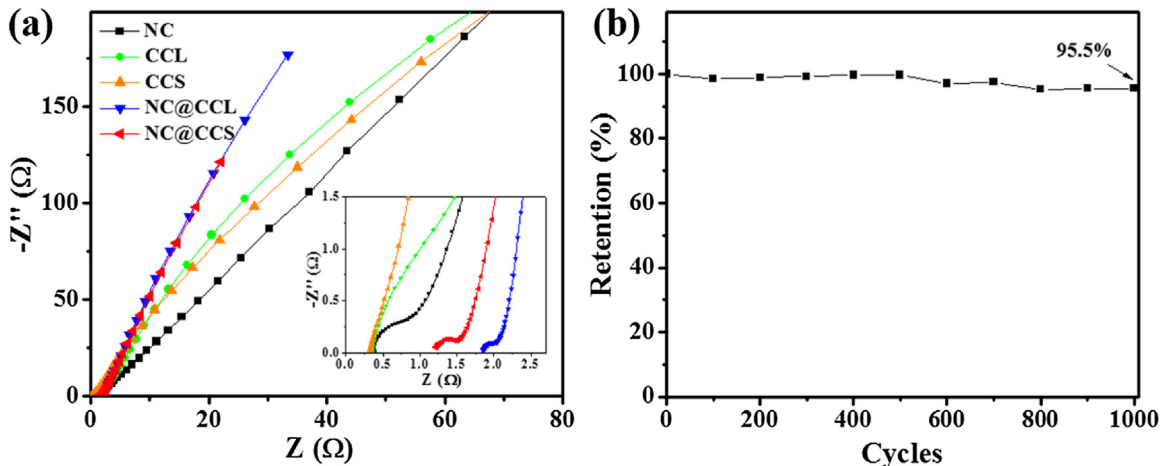


Fig. 6. (a) EIS Nyquist plots of the electrodes and (b) the evaluation of specific capacitance versus the number of cycles at 8 A g^{-1} .

the quasi-triangular CV curves of these two electrodes are similar to that of the NC, indicating poor capacitance performance. The specific capacitance of NC-8@CCS and NC-67@CCS were measured by GCD. The calculated specific capacitance is 62.6 F g^{-1} and 13.9 F g^{-1} , much smaller than that of NC@CCS. Furthermore, it can be seen from the EIS that the resistance of the two materials is larger than that of NC. This indicates that the ligands of benzimidazole (ZIF-7) plays a critical role in improving the SSA and EDLC performance, which is more conductively to form porous carbon with dense-

ring structure than other ligand without benzene ring (Wang et al., 2013). It can also see that the specific capacitance of NC-8@CCS is larger than that of NC-67@CCS. For the same ligand of ZIF-8 and ZIF-67, the center ion of Zn(II) is better than Co(II) in specific capacitance, which corresponding to the result of Yamauchi et al. (Jiang, Akita, Ishida, Haruta & Xu, 2011).

The above mentioned carbon cryogel materials showed remarkable improvement of capacitance performance, demonstrating the advantage of adding ZIF-7 into CL and CS cryogels. Specifically, it can

be explained by 1) As a hard template, ZIF-7 can efficiently improve the stability of cryogel and inhibit the agglomeration of cryogel during carbonization in high temperature; 2) Addition of ZIF-7 into cryogel can create a more compact structure, which decreases the pore volume after carbonization, and also supports suitable pore size for storage electrons; 3) ZIF-7 also supports more pyridine-nitrogen and graphite-nitrogen to cryogel, which could enhance the electrochemical performance of carbonized aerogels; 4) It is better to use ZIF-7 than other ZIFs, because the Zn(II) can induce the loss of carbon at high temperature, and the ligand of benzimidazole can form dense-ring structure to support more mesoporous to carbon cryogels.

4. Conclusion

In conclusion, we have designed and synthesized carbonized ZIF-7 composite cryogel materials. The resultant NC@CCL and NC@CCS showed the sandwich and coral structure microscopically. The materials exhibited suitable microspore contents of 34.37% and 30%, respectively, and they both showed an internal resistance lower than 2Ω . Thereby, NC@CCL and NC@CCS exhibited a high specific capacitance of 150.4 F g^{-1} and 173.1 F g^{-1} , respectively, which were much higher than those of the original materials. These results prove they are ideal potential supercapacitor electrode materials. Compared with NC-8@CCS and NC-67@CCS, it can be found that larger molecular weight of ZIFs ligand can lead to higher specific capacitance, and Zn(II) as central metal ion can achieve greater specific capacitance than Co(II) with the same ligand. The combination of ZIFs and carbon cryogels can effectively improve the conductivity and stability of carbon cryogels, the method can be further broaden the synthesis of other carbon composites derived from carbohydrates.

Acknowledgements

This research was supported by a grant from the National High Technology Research, Development Program of China (863 Program) (No. 2014AA06A513), National Natural Science Foundation of China (No. 51425405, 51608509) and China Postdoctoral Science Foundation Funded Project (2016M590670).

Appendix A. Supplementary data

Supplementary data associated with this article can be found, in the online version, at <http://dx.doi.org/10.1016/j.carbpol.2017.07.089>.

References

- Chaikittisilp, W., Hu, M., Wang, H., Huang, H. S., Fujita, T., Wu, K. C., et al. (2012). Nanoporous carbons through direct carbonization of a zeolitic imidazolate framework for supercapacitor electrodes. *Chemical Communications*, 48(58), 7259–7261.
- Du, X., Guo, P., Song, H., & Chen, X. (2010). Graphene nanosheets as electrode material for electric double-layer capacitors. *Electrochimica Acta*, 55(16), 4812–4819.
- Fazlifard, S., Mohammadi, T., & Bakhtiari, O. (2017). Chitosan/ZIF-8 mixed-matrix membranes for pervaporation dehydration of isopropanol. *Chemical Engineering & Technology*, 40(4), 648–655.
- Foresti, M. L., Vazquez, A., & Boury, B. (2017). Applications of bacterial cellulose as precursor of carbon and composites with metal oxide, metal sulfide and metal nanoparticles: A review of recent advances. *Carbohydrate Polymers*, 157, 447–467.
- Frindly, S., Primo, A., Ennajih, H., Qaiss, A. E. K., Bouhfid, R., Lahcini, M., et al. (2017). Chitosan-graphene oxide films and CO_2 -dried porous aerogel microspheres: Interfacial interplay and stability. *Carbohydrate Polymers*, 167, 297–305.
- Gao, Y. L., Wu, J. X., Zhang, W., Tan, Y. Y., Gao, J., Zhao, J. C., et al. (2014). The calcined zeolitic imidazolate framework-8 (ZIF-8) under different conditions as electrode for supercapacitor applications. *Journal of Solid State Electrochemistry*, 18(11), 3203–3207.
- Gao, X., Hai, X., Baigude, H., Guan, W., & Liu, Z. (2016). Fabrication of functional hollow microspheres constructed from mof shells: Promising drug delivery systems with high loading capacity and targeted transport. *Scientific Reports*, 6, 1–10.
- Hao, P., Zhao, Z., Tian, J., Li, H., Sang, Y., Yu, G., et al. (2014). Hierarchical porous carbon aerogel derived from bagasse for high performance supercapacitor electrode. *Nanoscale*, 6(20), 12120–12129.
- Hao, P., Zhao, Z., Leng, Y., Tian, J., Sang, Y., Boughton, R. I., et al. (2015). Graphene-based nitrogen self-doped hierarchical porous carbon aerogels derived from chitosan for high performance supercapacitors. *Nano Energy*, 15, 9–23.
- Jiang, H. L., Akita, T., Ishida, T., Haruta, M., & Xu, Q. (2011). Synergistic catalysis of Au@Ag core-shell nanoparticles stabilized on metal-organic framework. *Journal of the American Chemical Society*, 133(5), 1304–1306.
- Jiang, X., Sun, L. X., & Xu, F. (2016). ZIF-8 derived graphene-based nitrogen-doped porous carbons highly efficient supercapacitor electrodes. *Materials Science Forum*, 852, 829–834.
- Lang, X. Y., Hirata, A., Fujita, T., & Chen, M. W. (2011). Nanoporous metal/oxide hybrid electrodes for electrochemical supercapacitors. *Nature Nanotechnology*, 6(4), 232–236.
- Li, M., Liu, C., Cao, H., Zhao, H., Zhang, Y., & Fan, Z. (2014). KOH self-templating synthesis of three-dimensional hierarchical porous carbon materials for high performance supercapacitors. *Journal of Materials Chemistry A*, 2(36), 14844–14851.
- Liu, D., Li, Z., Zhu, Y., Li, Z., & Kumar, R. (2014). Recycled chitosan nanofibril as an effective Cu(II), Pb(II) and Cd(II) ionic chelating agent: Adsorption and desorption performance. *Carbohydrate Polymers*, 111(1), 469–476.
- Peng, S., Fan, L., Wei, C., Liu, X., Zhang, H., Xu, W., et al. (2017). Flexible polypyrrole/copper sulfide/bacterial cellulose nanofibrous composite membranes as supercapacitor electrodes. *Carbohydrate Polymers*, 157, 344–352.
- Qiu, S., Wu, L., Shi, G., Zhang, L., Chen, H., & Gao, C. (2010). Preparation and pervaporation property of chitosan membrane with functionalized multiwalled carbon nanotubes. *Industrial & Engineering Chemistry Research*, 49(22), 11667–11675.
- Snook, G. A., Kao, P., & Best, A. S. (2011). Conducting-polymer-based supercapacitor devices and electrodes. *Journal of Power Sources*, 196(1), 1–12.
- Tian, J., Peng, D., Wu, X., Li, W., Deng, H., & Liu, S. (2017). Electrodeposition of Ag nanoparticles on conductive polyaniline/cellulose aerogels with increased synergistic effect for energy storage. *Carbohydrate Polymers*, 156, 19–25.
- Wan, C., & Li, J. (2017). Synthesis and electromagnetic interference shielding of cellulose-derived carbon aerogels functionalized with $\alpha\text{-Fe}_2\text{O}_3$ and polypyrrole. *Carbohydrate Polymers*, 161, 158–165.
- Wang, Q., Xia, W., Guo, W., An, L., Xia, D., & Zou, R. (2013). Functional zeolitic-imidazolate-framework-templated porous carbon materials for CO_2 capture and enhanced capacitors. *Chemistry an Asian Journal*, 8(8), 1879–1885.
- Wei, J., Hu, Y., Liang, Y., Kong, B., Zhang, J., Song, J., et al. (2015). Nitrogen-doped nanoporous carbon/graphene nano-sandwiches: Synthesis and application for efficient oxygen reduction. *Advanced Functional Materials*, 25(36), 5768–5777.
- Wei, X., Wan, S., & Gao, S. (2016). Self-assembly-template engineering nitrogen-doped carbon aerogels for high-rate supercapacitors. *Nano Energy*, 28, 206–215.
- Yang, Y., Huang, Q., Niu, L., Wang, D., Yan, C., She, Y., et al. (2017). Waterproof, ultrahigh areal-capacitance: Wearable supercapacitor fabrics. *Advanced Materials*, 1606679, 1–9.
- Yao, J., & Wang, H. (2014). Zeolitic imidazolate framework composite membranes and thin films: synthesis and applications. *Chemical Society Reviews*, 43(13), 4470–4493.
- York, R., & York, R. (2012). Do alternative energy sources displace fossil fuels? *Nature Climate Change*, 2(6), 441–443.
- You, J., Li, M., Ding, B., Wu, X., & Li, C. (2017). Crab chitin-based 2D soft nanomaterials for fully biobased electric devices. *Advanced Materials*, 1606895, 1–8.
- Yu, Z., Tetard, L., Zhai, L., & Thomas, J. (2015). Supercapacitor electrode materials: Nanostructures from 0 to 3 dimensions. *Energy & Environmental Science*, 8(3), 702–730.
- Zhai, Y., Dou, Y., Zhao, D., Fulvio, P. F., Mayes, R. T., & Dai, S. (2012). Cheminform abstract: Carbon materials for chemical capacitive energy storage. *Advanced Materials*, 23(42), 4828–4850.
- Zhang, P., Sun, F., Shen, Z., & Cao, D. (2014). ZIF-derived porous carbon: A promising supercapacitor electrode material. *Journal of Materials Chemistry A*, 2(32), 12873–12880.
- Zhang, Y., Lin, B., Wang, J., Tian, J., Sun, Y., Zhang, X., et al. (2016). All-solid-state asymmetric supercapacitors based on ZnO quantum dots/carbon/CNTs and porous N-doped carbon/CNTs electrodes derived from a single ZIF-8/CNTs template. *Journal of Materials Chemistry A*, 4(26), 10282–10293.
- Zhou, Y., Guan, X., Zhou, H., Ramadoss, K., Adam, S., Liu, H., et al. (2016). Strongly correlated perovskite fuel cells. *Nature*, 534(7606), 231–234.
- Zhu, C. Z., & Dong, S. J. (2013). Recent progress in graphene-based nanomaterials as advanced electrocatalysts towards oxygen reduction reaction. *Nanoscale*, 5(5), 1753–1767.